

Structural position and oxidation state of nickel in SrTiO₃

Irina A. Sluchinskaya^{*,‡}, Alexander I. Lebedev^{*} and Alexei Erko[†]

^{*}Physics Department, Moscow State University
Leninskie gory, 119991 Moscow, Russia

[†]Helmholtz-Zentrum Berlin
Albert-Einstein-Str. 15, 12489 Berlin, Germany

[‡]irinasluch@nm.ru

Received 19 July 2013; Revised 2 October 2013; Accepted 14 November 2013; Published 13 December 2013

The properties of Ni-doped strontium titanate are studied using X-ray diffraction and XAFS spectroscopy. It is shown that regardless of the preparation conditions, the SrTi_{1-x}Ni_xO₃ solid solution and the NiTiO₃ phase are the most stable phases which can coexist. According to the EXAFS data, in the single-phase sample of SrTi_{0.97}Ni_{0.03}O₃, the Ni atoms substitute for the Ti ones and are on-center. The distortion of the oxygen octahedra is not observed. The XANES spectra analysis shows that the oxidation state of nickel in NiTiO₃ is 2+, and in the SrTi_{1-x}Ni_xO₃ solid solution it is close to 4+. It is shown that the strongest light absorption in doped samples is associated with the presence of tetravalent nickel in the SrTi_{1-x}Ni_xO₃ solid solution. This doping seems the most promising one for solar energy converters that exploit the bulk photovoltaic effect.

Keywords: XAFS spectroscopy; impurities; strontium titanate; solar energy conversion.

1. Introduction

The bulk photovoltaic effect consists in the occurrence of a photocurrent and very large photovoltages when illuminating homogeneous crystals having no inversion symmetry.¹ The idea of the practical application of this effect in ferroelectrics for solar energy conversion was discussed back in the 70s.² However, because of the short lifetime of photo-excited carriers, the quantum yield of this effect is generally small, and the idea was decided to be unproductive. In recent years, the interest to the ferroelectric oxides with the perovskite structure has revived because new ideas on how to increase the efficiency of solar energy converters based on the bulk photovoltaic effect have been proposed.^{3,4} The main disadvantage of the ferroelectric oxides is their relatively large bandgap, causing them to absorb only a small fraction of the solar radiation. Recent theoretical studies have shown that the substitution of Ti atoms at the *B* sites of the perovskite structure with divalent impurities having the *d*⁸ electron configuration (Ni, Pd, Pt), compensated by the oxygen vacancy, decreases the bandgap and the obtained perovskites are polar semiconductor oxides.^{5,6}

An additional interest to the study of the Ni impurity is associated with the results obtained from the recent experimental and theoretical studies of new materials — a recently synthesized PbNiO₃ which has a very high calculated spontaneous polarization⁷⁻⁹ and BiNiO₃ with unexpected oxidation states of nickel and bismuth atoms.¹⁰

In addition, the search for new magnetic off-center impurities in incipient ferroelectrics is still important because they can result in simultaneous emergence of the ferroelectricity and magnetic ordering and give rise to the magnetoelectric

interaction. Materials with these properties belong to multiferroics. SrTiO₃ doped with Mn at the *A* site is an example of such a material, in which a new type of magnetoelectric interaction was recently discovered.^{11,12} Ni-doped samples could be another example.

Since the doping impurity can enter several different sites in the perovskite structure and stay in them in different oxidation states, the aim of this work was to study the structural position and the oxidation state of the Ni impurity in SrTiO₃ prepared under different conditions using XAFS spectroscopy. We planned to check the possibility of preparing samples doped with divalent Ni at the *B* site, to evaluate the possibility of incorporating the Ni impurity into the *A* site, and to establish a correlation between the optical properties of the samples, on the one hand, and the structural position and the oxidation state of the Ni impurity, on the other hand. The choice of SrTiO₃ was dictated by the fact that earlier we have studied the structural position and the oxidation state of a number of 3*d* elements in SrTiO₃ (Mn,^{13,14} Co,¹⁵ Fe¹⁶), and their combined analysis can allow to find new promising impurities for solar energy converters.

2. Samples and Experimental Techniques

Ni-doped samples of SrTiO₃ with the impurity concentration of 2–3% and different deviation from stoichiometry were prepared by the solid-state reaction method. The starting materials were SrCO₃, nanocrystalline TiO₂, and Ni (CH₃COO)₂·4H₂O. The components were weighed in proper proportions, mixed, ground in acetone, and calcined in air at 1100°C for 8 h. The calcined powders were ground once

more and annealed again under the same conditions. Some of the samples were additionally calcined in air at 1500°C for 2 h. The composition of the samples was deliberately deviated from stoichiometry (excess titanium or excess strontium) in order to incorporate the impurity into the *A* or *B* site of the perovskite structure.

The reference compounds NiO, NiTiO₃, and BaNiO_{3-δ} used for determination of the oxidation state of Ni in SrTiO₃ were prepared as follows. NiO was obtained by thermal decomposition of Ni(CH₃COO)₂·4H₂O. Two other samples were prepared by the solid-state reaction method in air: the NiTiO₃ sample was obtained from Ni(CH₃COO)₂·4H₂O and TiO₂ at 1100°C, the BaNiO_{3-δ} sample was prepared from BaO₂ and NiO at 650°C. The phase composition of the samples was controlled by X-ray diffraction.

Extended X-ray absorption fine structure (EXAFS) and X-ray absorption near-edge structure (XANES) spectra were obtained at KMC-2 station of the BESSY synchrotron radiation source (the beam energy 1.7 GeV; the beam current up to 290 mA) at the Ni *K*-edge (8340 eV) at 300 K. The radiation was monochromatized by a double-crystal Si_{1-x}Ge_x(111) monochromator. Spectra were collected in fluorescence mode. The radiation intensity incident on the sample (*I*₀) was measured by an ionization chamber; the fluorescence intensity (*I*_f) was measured by a silicon energy-dispersive RÖNTEC X-flash detector with 10 mm² active area.

Isolation of the oscillating EXAFS function $\chi(k)$ from the fluorescence excitation spectra $\mu(E) = I_f/I_0$ (where *E* is the X-ray photon energy) was performed in the traditional way.^{17,18} After subtracting the pre-edge background, splines were used to extract the monotonic atomic part of the spectrum $\mu_0(E)$ and then the dependence of $\chi = (\mu - \mu_0)/\mu_0$ was calculated as a function of the photoelectron wave vector $k = (2m(E - E_0)/\hbar^2)^{1/2}$. The energy origin, *E*₀, was taken to be the position of the inflection point on the absorption edge. For each sample three spectra were recorded, they were then independently processed, and the resulting $\chi(k)$ curves finally averaged.

Direct and inverse Fourier transforms with modified Hanning windows were used to extract the information about the first three shells from the obtained $\chi(k)$ curves. The distances *R*_{*j*} and Debye–Waller factors σ_j^2 for *j*th shell (*j* = 1–3) as well as the energy origin correction *dE*₀ were simultaneously varied to obtain the minimum root-mean-square deviation between the experimental and calculated $k^2\chi(k)$ curves. The coordination numbers were considered fixed for a given structural model. The number of adjustable parameters (8) was usually about a half of the number of independent data points $N_{\text{ind}} = 2\Delta k\Delta R/\pi \approx 16$.

The single- and multiple-scattering amplitudes and phase shifts, the central atom phase shift, and the photoelectron mean free path as a function of *k*, needed to calculate the theoretical curves $\chi(k)$, were computed using the FEFF6 software.¹⁹

EXAFS spectra were also analyzed with a widely used IFEFFIT software package.²⁰ Isolation of the experimental EXAFS function was carried out using the ATHENA program and its fitting to the theoretical curve calculated for a given structural model was performed using the ARTEMIS program. In this approach, the amplitudes and phase shifts for all single- and multiple-scattering paths were also calculated using the FEFF6 software. The results obtained by two different data analysis approaches agreed well.

3. Results

3.1. X-ray data

The diffraction patterns of all investigated samples are shown in Fig. 1. It is seen that the SrTi_{0.97}Ni_{0.03}O₃ sample annealed at 1500°C is the only single-phase sample which has a cubic perovskite structure; for other samples, additional reflections were observed on the diffraction patterns. For the SrTi_{0.97}Ni_{0.03}O₃ and Sr_{0.98}Ni_{0.02}TiO₃ samples annealed at 1100°C, along with the reflections characteristic of the perovskite phase, additional reflections indicating a small amount of TiO₂ and, presumably, NiTiO₃ were observed. The identification of a possible NiO phase was complicated by the closeness of its reflections to the position of NiTiO₃ reflections. In addition, stronger lines of the Ruddlesden–Popper phases Sr₃Ti₂O₇ and Sr₄Ti₃O₁₀ were observed in the SrTi_{0.97}Ni_{0.03}O₃ sample annealed at 1100°C. In the Sr_{0.98}Ni_{0.02}TiO₃ sample annealed at 1500°C the only additional phase, NiTiO₃, was found.

Since barium nickelate BaNiO_{3-δ} is a defective phase with the δ value depending on the preparation conditions, its lattice parameters dependence on the δ value²¹ was used to determine the actual oxygen content in our BaNiO_{3-δ}

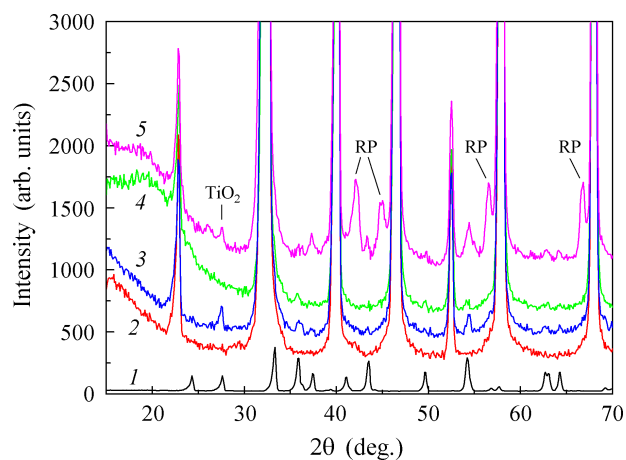


Fig. 1. (Color online) Diffraction patterns of samples: (1) NiTiO₃, (2) SrTi_{0.97}Ni_{0.03}O₃ sample annealed at 1500°C, (3) Sr_{0.98}Ni_{0.02}TiO₃ sample annealed at 1100°C, (4) Sr_{0.98}Ni_{0.02}TiO₃ sample annealed at 1500°C, and (5) SrTi_{0.97}Ni_{0.03}O₃ sample annealed at 1100°C. Reflections of TiO₂ and Ruddlesden–Popper (RP) phases are also indicated.

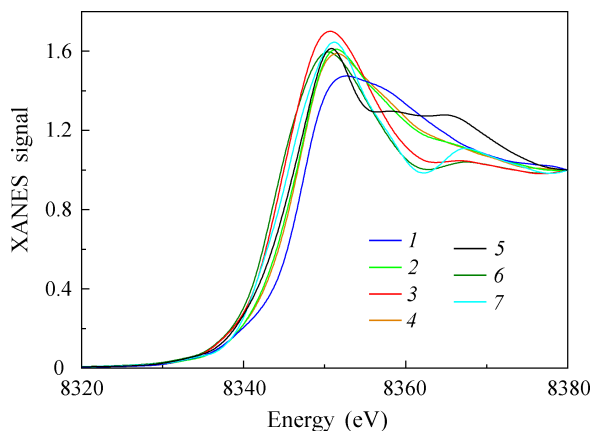


Fig. 2. (Color online) XANES spectra for SrTiO₃(Ni) samples and nickel reference compounds: (1) SrTi_{0.97}Ni_{0.03}O₃ sample annealed at 1500°C, (2) SrTi_{0.97}Ni_{0.03}O₃ sample annealed at 1100°C, (3) Sr_{0.98}Ni_{0.02}TiO₃ sample annealed at 1500°C, (4) Sr_{0.98}Ni_{0.02}TiO₃ sample annealed at 1100°C, (5) BaNiO_{3-δ}, (6) NiTiO₃ and (7) NiO.

sample. The hexagonal lattice parameters of $a = 5.568 \pm 0.001 \text{ \AA}$, $c = 4.838 \pm 0.001 \text{ \AA}$ in our sample correspond to $\delta \approx 0.4$.

3.2. XANES data analysis

To determine the oxidation state of the Ni impurity in SrTiO₃, the position of the absorption edge in XANES spectra of the samples was compared with the edge positions in the reference compounds. XANES spectra of all studied samples and three reference compounds are shown in Fig. 2.

Comparison of the spectra of the Sr_{0.98}Ni_{0.02}TiO₃ sample annealed at 1500°C with the spectra of cubic NiO and rhombohedral NiTiO₃ (with the ilmenite structure) shows that the absorption edges in these samples are very close. So, we conclude that the Ni impurity in the sample under consideration is in the 2+ oxidation state. The absorption edges of the SrTi_{0.97}Ni_{0.03}O₃ and Sr_{0.98}Ni_{0.02}TiO₃ samples annealed at 1100°C are close to the absorption edge of the BaNiO_{3-δ} reference compound. In the single-phase SrTi_{0.97}Ni_{0.03}O₃ sample annealed at 1500°C, the absorption edge is shifted to even higher energies (by 2.5 eV as compared to NiO, by 2.9 eV as compared to NiTiO₃, and by 1.3 eV as compared to BaNiO_{3-δ}).

3.3. EXAFS data analysis

To determine the structural position of the Ni impurity, EXAFS spectra were analyzed. A typical EXAFS spectrum $k^2\chi(k)$ for the single-phase SrTi_{0.97}Ni_{0.03}O₃ sample annealed at 1500°C and its best theoretical fit (which takes into account the multiple-scattering effects) are shown in Fig. 3.

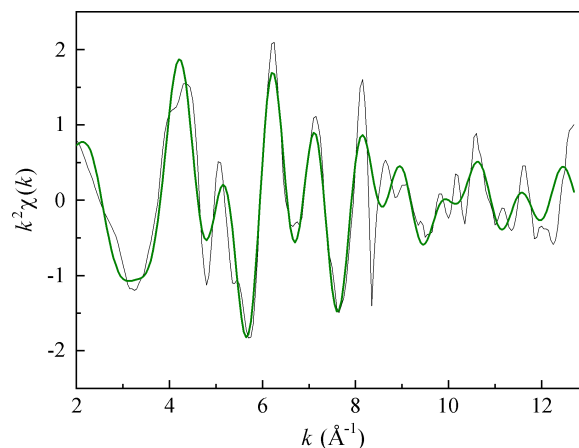


Fig. 3. (Color online) EXAFS spectrum recorded at the Ni K-edge at 300 K for SrTi_{0.97}Ni_{0.03}O₃ sample annealed at 1500°C (thin black line) and its best theoretical fit (thick green line).

The best agreement between the calculated and experimental data was obtained in the model in which Ni atoms substitute for Ti atoms in SrTiO₃. The interatomic distances and Debye–Waller factors for three nearest shells are given in Table 1. Small values of the Debye–Waller factor for the first and second shells, which are typical for the thermal vibrations in perovskites at 300 K, enable to draw two conclusions: (1) the off-centering of Ni atoms at the B sites can be excluded and (2) there is no distortion of the oxygen octahedra around the impurity atoms.^a

The analysis of the EXAFS spectra helped us to determine the composition of the second phase precipitating in the Sr_{0.98}Ni_{0.02}TiO₃ sample annealed at 1500°C. Although the distances and the coordination numbers for the first shell of Ni are close in NiO and NiTiO₃, the coordination numbers for the second shell in these compounds differ by three times. A comparison of the Fourier transforms of the EXAFS spectra for the sample under consideration and two reference compounds, NiTiO₃ and NiO, shows a better agreement of its spectrum with that of NiTiO₃ (Fig. 4). This means that among two possible phases, NiTiO₃ and NiO, the second phase in our samples is the NiTiO₃ one.

As concerns to two-phase SrTi_{0.97}Ni_{0.03}O₃ and Sr_{0.98}Ni_{0.02}TiO₃ samples annealed at 1100°C, the comparison of their EXAFS spectra with the EXAFS spectrum of the single-phase solid solution and the EXAFS spectrum of NiTiO₃ shows that the spectra of the samples under discussion may be represented as a superposition of the spectra of NiTiO₃ and of the solid solution in a ratio close to 1:1.

The optical properties of the samples are consistent with the data obtained above. The Sr_{0.98}Ni_{0.02}TiO₃ sample

^aThe sensitivity of the Debye–Waller factor to small distortions of the oxygen octahedra can be illustrated by the EXAFS data for NiTiO₃. In this compound, there are two Ni–O distances in the first shell which differ by $\sim 0.07 \text{ \AA}$; such a small distortion increases the Debye–Waller factor to $0.0073 \pm 0.0012 \text{ \AA}^2$.

Table 1. Structural parameters obtained from the data analysis of the EXAFS spectra for $\text{SrTi}_{0.97}\text{Ni}_{0.03}\text{O}_3$ sample annealed at 1500°C (R_i is the distance to the i th shell, σ_i^2 is the Debye–Waller factor for this shell).

Shell	R_i (Å)	σ_i^2 (Å ²)	Atom
1	1.914 ± 0.004	0.0035 ± 0.0006	O
2	3.342 ± 0.006	0.0084 ± 0.0007	Sr
3	3.877 ± 0.004	0.0053 ± 0.0005	Ti

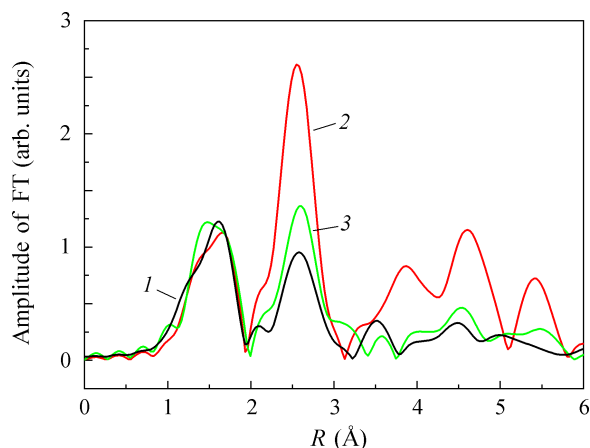


Fig. 4. (Color online) Comparison of Fourier transforms of the EXAFS $k^2\chi(k)$ spectra obtained for (1) $\text{Sr}_{0.98}\text{Ni}_{0.02}\text{TiO}_3$ sample annealed at 1500°C and for (2) NiO and (3) NiTiO_3 reference compounds.

annealed at 1500°C had a light brown color; the $\text{SrTi}_{0.97}\text{Ni}_{0.03}\text{O}_3$ and $\text{Sr}_{0.98}\text{Ni}_{0.02}\text{TiO}_3$ samples annealed at 1100°C were dark brown; the $\text{SrTi}_{0.97}\text{Ni}_{0.03}\text{O}_3$ sample annealed at 1500°C had an almost black color. Thus, the color of the samples reflects the relative amounts of black $\text{SrTi}_{1-x}\text{Ni}_x\text{O}_3$ and yellow NiTiO_3 phases in the samples.

4. Discussion

Combined analysis of X-ray and EXAFS data shows that the $\text{SrTi}_{0.97}\text{Ni}_{0.03}\text{O}_3$ sample annealed at 1500°C is the single-phase solid solution in which the Ni atoms substitute for the Ti atoms at the B sites and are on-center. This means that the solubility of nickel at the B sites in SrTiO_3 exceeds 3% at 1500°C . In the sample with a nominal composition of $\text{SrTi}_{0.97}\text{Ni}_{0.03}\text{O}_3$ annealed at 1100°C , the appearance of reflections of NiTiO_3 and of the Ruddlesden–Popper phases indicates that a part of Ni atoms is spent on the NiTiO_3 formation, while the other part remains at the B sites. As a result, some untapped Sr atoms form the SrO planes which embed into the perovskite structure and form the $\text{Sr}_3\text{Ti}_2\text{O}_7$ and $\text{Sr}_4\text{Ti}_3\text{O}_{10}$ phases.

When trying to incorporate Ni atoms into the A sites of SrTiO_3 at 1500°C (the samples with a nominal

composition of $\text{Sr}_{0.98}\text{Ni}_{0.02}\text{TiO}_3$), the precipitation of the NiTiO_3 second phase occurs. The concentration of nickel in the solid solution phase is small, as it follows from the EXAFS data and the sample color. In contrast, when annealing the $\text{Sr}_{0.98}\text{Ni}_{0.02}\text{TiO}_3$ sample at a lower temperature (1100°C), nickel in the sample is in a mixture of NiTiO_3 and $\text{SrTi}_{1-x}\text{Ni}_x\text{O}_3$ solid solution as follows from the XANES data, EXAFS data, and the sample color. The precipitation of a small portion of TiO_2 confirms the incorporation of Ni into SrTiO_3 (the appearance of TiO_2 is a consequence of removing of some Ti atoms from the B sites when doping strontium titanate with nickel).

As concerns to the appearance of the TiO_2 phase in the $\text{SrTi}_{0.97}\text{Ni}_{0.03}\text{O}_3$ sample annealed at 1100°C , we suppose that its appearance is possible for kinetic reasons. The formation of the solid solution occurs as a result of a chain of chemical reactions in which the NiTiO_3 phase initially formed at $\sim 750^\circ\text{C}$ from NiO and TiO_2 reacts with excess SrO resulted from the thermal decomposition of SrCO_3 at $\sim 1000^\circ\text{C}$ to produce $\text{SrNiO}_{2.5} + \text{TiO}_2$ as intermediate phases. This reaction is quite slow (the preparation of $\text{SrNiO}_{2.5}$ usually takes 48 h at 1000°C , Ref. 22). As a result, in the samples annealed at 1100°C for 16 h, a mixture of the solid solution, NiTiO_3 , and TiO_2 is observed. At higher annealing temperature, the kinetic processes are faster, the reaction completes, and the composition of the samples is fully controlled by the deviation from stoichiometry.

Therefore, the stable phases in the samples are the single-phase $\text{SrTi}_{1-x}\text{Ni}_x\text{O}_3$ solid solution and NiTiO_3 ; their ratio depends on the deviation from stoichiometry and the annealing temperature. Nickel cannot be incorporated into the A sites of strontium titanate. The low stability of Ni at the A site of SrTiO_3 is apparently related to the large difference in the ionic radii of Ni^{2+} and Sr^{2+} . The 12-fold coordination is not typical for nickel; for the coordination number of 6, the ionic radius of Ni^{2+} (0.69 \AA) is much less than that of Sr^{2+} (1.18 \AA).²³

The XANES data, which were used to determine the oxidation state of nickel, are fully consistent with X-ray and EXAFS data. In the sample with a nominal composition of $\text{Sr}_{0.98}\text{Ni}_{0.02}\text{TiO}_3$ annealed at 1500°C , in which nickel is in the NiTiO_3 phase, the oxidation state of Ni coincides with its oxidation state in NiO and NiTiO_3 and is $2+$. In the single-phase $\text{SrTi}_{0.97}\text{Ni}_{0.03}\text{O}_3$ sample annealed at 1500°C , the shift of the absorption edge with respect to NiTiO_3 is maximum and is about twice the shift between the reference compounds NiTiO_3 and $\text{BaNiO}_{3-\delta}$. If, following Ref. 21, we start from the number of ions, their nominal charge, and the $\delta \approx 0.4$ value determined from the lattice parameters, the average oxidation state of nickel in $\text{BaNiO}_{3-\delta}$ is $(4 - 2\delta) \approx 3.2$. Then, according to the shift of the absorption edge in $\text{SrTi}_{0.97}\text{Ni}_{0.03}\text{O}_3$ sample annealed at 1500°C , the oxidation state of nickel in it should be close to $4+$. For the $\text{SrTi}_{0.97}\text{Ni}_{0.03}\text{O}_3$ and $\text{Sr}_{0.98}\text{Ni}_{0.02}\text{TiO}_3$ samples annealed at 1100°C , which are the mixture of two nickel-containing

phases in proportion close to 1:1, the position of the absorption edge is intermediate between those in two stable phases and is close to the position of the absorption edge in $\text{BaNiO}_{3-\delta}$ (about 3+).

It should be noted that the question about the oxidation state of Ni in $\text{SrTi}_{0.97}\text{Ni}_{0.03}\text{O}_3$ is not so simple. The discussion about the oxidation state of Ni in $\text{BaNiO}_{3-\delta}$ is still going on, in particular, the doubts were expressed²⁴ about the validity of its formal determination based on the number of ions and their nominal charges. In the cited work, the data of Mössbauer spectroscopy for BaNiO_3 indicated the Ni oxidation state close to 4+, whereas the photoelectron spectroscopy gave a value close to 3+. The authors of Ref. 24 suggested a model in which Ni is trivalent and its charge is compensated by a hole bound by one or two negative oxygen ions. Within this model, the Ni oxidation state determined from the absorption edge shift in our $\text{SrTi}_{0.97}\text{Ni}_{0.03}\text{O}_3$ solid solution should be closer to 3+. This explanation, however, contradicts the fact that our EXAFS data analysis revealed no distortion of the oxygen octahedra, whereas the localization of a hole at one or two oxygen ions should cause its distortion.

At the same time, the experimental study of XANES spectra of Li_xNiO_2 compound used in lithium batteries have shown that a variation in the degree of intercalation x changes the Ni oxidation state from 2+ to 4+ and shifts the absorption edge in XANES spectra by ~ 3.5 eV.²⁵ This shift is close to the shift of 2.9 eV observed in our spectra between NiTiO_3 and the $\text{SrTi}_{0.97}\text{Ni}_{0.03}\text{O}_3$ sample annealed at 1500°C. Moreover, the interatomic Ni–O distance (1.914 Å) obtained from our EXAFS measurements is less than the sum of the ionic radii of Ni^{3+} and O^{2-} ($0.56 + 1.4 = 1.96$ Å) and is closer to the sum of the ionic radii of Ni^{4+} and O^{2-} ($0.48 + 1.4 = 1.88$ Å). Yet another argument in favor of tetravalent nickel can be the small value of the Debye–Waller factor σ_1^2 , which indicates the absence of the Ni displacement from the *B* site in the $\text{SrTi}_{0.97}\text{Ni}_{0.03}\text{O}_3$ solid solution. If the nickel atom in this phase was in the Ni^{3+} oxidation state, it required to be charge-compensated by the oxygen vacancy located nearby the impurity atom (such $\text{Ni}^{3+}-V_{\text{O}}$ axial centers with the Ni displacement from the center of the octahedron up to ~ 0.3 Å have been observed in electron spin resonance (ESR) spectra).^{26,27} However, our EXAFS measurements did not reveal noticeable distortion of the oxygen octahedra surrounding the Ni atom.

It should be noted that the EXAFS data analysis of the $\text{SrTi}_{0.97}\text{Ni}_{0.03}\text{O}_3$ sample annealed at 1500°C revealed a reduced value of 4.90 ± 0.34 for the coordination number for the first shell of Ni. There are two possible explanation of this fact. First, it can be an evidence for the existence of a small amount of $\text{Ni}^{3+}-V_{\text{O}}$ complexes. The coordination number for these complexes is effectively reduced to 4 because one of the oxygen atoms is missing and the other one is located at a different distance compared to four remaining O atoms and does not contribute much to the EXAFS signal. This explanation agrees with the reduced shift of the absorption edge in our sample with respect to the Ni^{4+} state in Li_xNiO_2 . Another

explanation is the existence of a small amount of the NiTiO_3 phase located at the grain boundaries; the experiment shows that the contamination with this phase strongly decreases the coordination number because of out-of-phase EXAFS oscillations in two nickel-containing phases.

Nevertheless, we think that the oxidation state of Ni at the *B* site in SrTiO_3 is close to 4+; this disagrees with the suggestion made earlier^{5,6} that Ni is in the 2+ oxidation state in the related ferroelectric PbTiO_3 . Although the question about the actual oxidation state of Ni in the latter material should be tested experimentally, our findings indicate that the strong light absorption in Ni-doped SrTiO_3 is associated with the tetravalent nickel.

From the viewpoint of possible application of doped perovskites in solar energy conversion it is interesting to compare the properties of SrTiO_3 doped with nickel and with other 3d elements.^{13–16} The absorption spectra of doped samples are systematically shifted to the infrared region with increasing atomic number from Mn to Ni: manganese-doped samples are greenish brown, iron-doped samples are brown, cobalt-doped samples are dark brown, and Ni gives an almost black color to the samples. Thus, for creating samples that strongly absorb light in the whole visible region, the nickel doping seems the most promising. Intense absorption in the samples suggests that it is associated with charge-transfer transitions.

Interestingly, the small value of the Debye–Waller factor for the first shell ($\sigma_1^2 \approx 0.0035$ Å²) also excludes the possibility of Jahn–Teller instability of the Ni^{4+} ion in SrTiO_3 , which is possible for the octahedral d^6 configuration. In Li_xNiO_2 , the Jahn–Teller instability of Ni^{4+} manifests itself in the distorted oxygen octahedra with Ni–O bond lengths of 1.88 and 2.08 Å. In the EXAFS spectra, this distorted environment should be observed as one O shell with an average interatomic distance of 1.947 Å and a static Debye–Waller factor of 0.009 Å². The experimental value of σ_1^2 in $\text{SrTiO}_3(\text{Ni})$ is much lower than the value estimated for Jahn–Teller-distorted environment.

The interpretation of our data on the oxidation state of nickel in SrTiO_3 differs much from the results of earlier studies. The comparison with the data of Ref. 28, in which $\text{SrTiO}_3(\text{Ni})$ samples were also studied by XAFS technique, shows that the XANES and EXAFS spectra obtained in our work and in Ref. 28 are qualitatively different. For example, in Ref. 28 the shift of the absorption edge in $\text{SrTiO}_3(\text{Ni})$ with respect to NiO was only 1.1 eV (in our samples it is 2.5 eV). Moreover, even the color of the samples is different (beige in Ref. 28 and almost black in our work). We believe that these differences in the properties of the samples result from the different methods of their preparation (solid-state reaction method in our case and hydrothermal synthesis at 150°C in Ref. 28). In Refs. 26 and 27, single crystals of $\text{SrTiO}_3(\text{Ni})$ were investigated by electron spin resonance. In these works, the ESR spectra associated with axial $\text{Ni}^{3+}-V_{\text{O}}$ complexes were systematically observed along with the ESR spectra which were attributed to the “cubic” Ni^{2+} and Ni^{3+}

centers.²⁶ Unfortunately, no arguments on the basis of which the oxidation state of the Ni impurity was identified were presented in Ref. 26, and a possible interpretation of the ESR spectra as the spectra of Ni⁴⁺ was not discussed.

5. Conclusion

The study of Ni-doped SrTiO₃ using X-ray diffraction and XAFS spectroscopy enabled to draw the following conclusions:

1. The preparation conditions of single-phase Ni-doped SrTiO₃ samples with the impurity concentration up to at least 3% have been found. When incorporating the impurity into the A sites, the NiTiO₃ second phase was precipitated. Regardless of the preparation conditions, the SrTi_{1-x}Ni_xO₃ solid solution and NiTiO₃ phase are the most stable phases which can coexist.
2. EXAFS analysis showed that in the single-phase SrTi_{0.97}Ni_{0.03}O₃ sample, the Ni atoms substitute for the Ti atoms and are on-center. The distortion of the oxygen octahedra, which could occur because of the Ni off-centering or the existence of the oxygen vacancies in the Ni environment, was not detected. The reduced value of the coordination number for the first shell was explained by the presence of a small amount of Ni³⁺-V_O complexes and the NiTiO₃ phase at the grain boundaries.
3. XANES analysis showed that in NiTiO₃ the oxidation state of Ni is 2+ and in the SrTi_{1-x}Ni_xO₃ solid solution it is close to 4+.
4. The strongest light absorption in doped samples is associated with the presence of tetravalent nickel in the SrTi_{1-x}Ni_xO₃ solid solution. This doping seems to be the most promising for solar energy converters that exploit the bulk photovoltaic effect.

In the future, we plan to perform similar experiments on the ferroelectric BaTiO₃ doped with 3d elements in order to test the feasibility of obtaining the polar material with similar optical and physical properties, in which the bulk photovoltaic effect can be observed for photons in the whole spectrum of solar radiation.

Acknowledgments

This work was supported by Russian Foundation for Basic Research (Grant No. 13-02-00724). I. A. S. and A. I. L. are grateful to Russian-German laboratory for hospitality and financial support during their stay at BESSY.

References

¹B. I. Sturman and V. M. Fridkin, *Photogalvanic Effect in Media without the Inversion Center and Related Phenomena* (Nauka, Moscow, 1992).

- ²A. M. Glass, D. von der Linde and T. J. Negran, High-voltage bulk photovoltaic effect and the photorefractive process in LiNbO₃, *Appl. Phys. Lett.* **25**, 233 (1974).
- ³M. Qin, K. Yao and Y. C. Liang, High efficient photovoltaics in nanoscaled ferroelectric thin films, *Appl. Phys. Lett.* **93**, 122904 (2008).
- ⁴M. Alexe and D. Hesse, Tip-enhanced photovoltaic effects in bismuth ferrite, *Nat. Commun.* **2**, 256 (2011).
- ⁵J. W. Bennett, I. Grinberg and A. M. Rappe, New highly polar semiconductor ferroelectrics through d⁸ cation-o vacancy substitution into PbTiO₃: A theoretical study, *J. Am. Chem. Soc.* **130**, 17409 (2008).
- ⁶G. Y. Gou, J. W. Bennett, H. Takenaka and A. M. Rappe, Post density functional theoretical studies of highly polar semiconductive Pb(Ti_{1-x}Ni_x)O_{3-x} solid solutions: Effects of cation arrangement on band gap, *Phys. Rev. B* **83**, 205115 (2011).
- ⁷Y. Inaguma, M. Yoshida, T. Tsuchiya, A. Aimi, K. Tanaka, T. Katsumata and D. Mori, High-pressure synthesis of novel lithium niobate-type oxides, *J. Phys.: Conf. Ser.* **215**, 012131 (2010).
- ⁸Y. Inaguma, K. Tanaka, T. Tsuchiya, D. Mori, T. Katsumata, T. Ohba, K.-I. Hiraki, T. Takahashi and H. Saitoh, Synthesis, structural transformation, thermal stability, valence state, and magnetic and electronic properties of PbNiO₃ with perovskite- and LiNbO₃-type structures, *J. Am. Chem. Soc.* **133**, 16920 (2011).
- ⁹X. F. Hao, A. Stroppa, S. Picozzi, A. Filippetti and C. Franchini, Exceptionally large room-temperature ferroelectric polarization in the PbNiO₃ multiferroic nickelate: First-principles study, *Phys. Rev. B* **86**, 014116 (2012).
- ¹⁰M. Azuma, S. Carlsson, J. Rodgers, M. G. Tucker, M. Tsujimoto, S. Ishiwata, S. Isoda, Y. Shimakawa, M. Takano and J. P. Attfield, Pressure-induced intermetallic valence transition in BiNiO₃, *J. Am. Chem. Soc.* **129**, 14433 (2007).
- ¹¹V. V. Shvartsman, S. Bedanta, P. Borisov, W. Kleemann, A. Tkach and P. M. Vilarinho, (Sr, Mn)TiO₃: A magnetoelectric multiglass, *Phys. Rev. Lett.* **101**, 165704 (2008).
- ¹²W. Kleemann, S. Bedanta, P. Borisov, V. V. Shvartsman, S. Miga, J. Dec, A. Tkach and P. M. Vilarinho, Multiglass order and magnetoelectricity in Mn²⁺ doped incipient ferroelectrics, *Eur. Phys. J. B* **71**, 407 (2009).
- ¹³A. I. Lebedev, I. A. Sluchinskaya, A. Erko and V. F. Kozlovskii, Direct evidence for off-centering of Mn impurity in SrTiO₃, *JETP Lett.* **89**, 457 (2009).
- ¹⁴I. A. Sluchinskaya, A. I. Lebedev and A. Erko, Local environment and oxidation state of a Mn impurity in SrTiO₃ determined from XAFS data, *Bull. Russ. Acad. Sci.: Phys.* **74**, 1235 (2010).
- ¹⁵I. A. Sluchinskaya, A. I. Lebedev and A. Erko. *The 19th All-Russian Conf. Physics of Ferroelectrics*, Moscow (2011), Abstract book (2011), p. 116.
- ¹⁶I. A. Sluchinskaya, A. I. Lebedev, V. F. Kozlovskii and A. Erko, *The 8th National Conf. "X-ray, synchrotron radiation, neutrons, and electrons for studying nanosystems and materials"*, Moscow (2011), Abstract book (2011), p. 347.
- ¹⁷A. I. Lebedev, I. A. Sluchinskaya, V. N. Demin and I. Munro, EXAFS studies of the influence of impurities on the phase transition in GeTe, *Izv. Akad. Nauk SSSR, Ser. Fiz.* **60**, 46 (1996).
- ¹⁸A. I. Lebedev, I. A. Sluchinskaya, V. N. Demin and I. H. Munro, Off-centering of Pb and Sn impurities in GeTe, *Phys. Rev. B* **55**, 14770 (1997).

- ¹⁹FEFF project home page, <http://leonardo.phys.washington.edu/feff/>. URL <http://leonardo.phys.washington.edu/feff/>.
- ²⁰IFEFFIT project home page, <http://cars9.uchicago.edu/ifeffit/>. URL <http://cars9.uchicago.edu/ifeffit/>.
- ²¹M. Arjomand and D. J. Machin, Oxide chemistry. Part I. Ternary oxides containing nickel in oxidation states II, III, and IV, *J. Chem. Soc., Dalton Trans.*, 1055 (1975).
- ²²Y. Takeda, T. Hashino, H. Miyamoto, F. Kanamaru, S. Kume and M. Koizumi, Synthesis of SrNiO₃ and related compound, Sr₂Ni₂O₅, *J. Inorg. Nucl. Chem.* **34**, 1599 (1972).
- ²³R. D. Shannon, Revised effective ionic radii and systematic studies of interatomic distances in halides and chalcogenides, *Acta Cryst. A* **32**, 751 (1976).
- ²⁴R. Gottschall, R. Schöllhorn, M. Muhler, N. Jansen, D. Walcher and P. Gülich, Electronic state of nickel in barium nickel oxide, BaNiO₃, *Inorg. Chem.* **37**, 1513 (1998).
- ²⁵A. N. Mansour and C. A. Melendres, Analysis of X-ray absorption spectra of some nickel oxycompounds using theoretical standards, *J. Phys. Chem. A* **102**, 65 (1998).
- ²⁶K. A. Müller, W. Berlinger and R. S. Rubins, Observation of two charged states of a nickel-oxygen vacancy pair in SrTiO₃ by paramagnetic resonance, *Phys. Rev.* **186**, 361 (1969).
- ²⁷S.-Y. Wu, J.-Z. Lin, Q. Fu and H.-M. Zhang, Investigations on the impurity displacements and the *g* factors of the two tetragonal Ni³⁺ centres in SrTiO₃, *Phys. Scripta.* **75**, 147 (2007).
- ²⁸A. M. Beale, M. Paul, G. Sankar, R. J. Oldman, C. R. A. Catlow, S. French and M. Fowles, Combined experimental and computational modelling studies of the solubility of nickel in strontium titanate, *J. Mater. Chem.* **19**, 4391 (2009).